Electron beam induced current in photovoltaics with high recombination

Paul Haney[1], Heayoung Yoon[1,2], and Nikolai Zhitenev[1]

1. Center for Nanoscale Science and Technology, National Institute of Standards and Technology, Gaithersburg, Maryland 20899-6202, USA
2. Maryland NanoCenter, University of Maryland, College Park, MD 20742, USA

***Abstract*—A model for interpreting electron beam induced current (EBIC) measurements is presented, which applies when recombination within the depletion region is substantial. This model is motivated by cross-sectional EBIC experiments on CdS-CdTe photovoltaic cells (prepared by cleaving, or focused ion beam milling). The experimental results clearly show that the maximum efficiency of carrier collection is less than 100 % and varies throughout the depletion region, contrary to the assumptions of most models used to interpret EBIC data. We describe a model which relaxes these assumptions by including recombination in the depletion region. We find that our model can reproduce experimental results only if the mobility-lifetime product $\mu\tau$ is spatially varying within the depletion region.**

***Index Terms*—Electron beam induced current, CdTe**

Quantitative determination of electronic properties at high spatial resolution is crucial for the development of high efficiency solar cells. Electron beam induced current (EBIC) is a powerful technique in which electron-hole pairs are created in proximity to an exposed surface, and the carrier collection efficiency is measured as a function of excitation position [1]. EBIC has enjoyed longstanding use as a diagnostic tool for measuring key material properties such as the minority carrier diffusion length. However, for complex polycrystalline materials such as CdTe, EBIC signals can be difficult to interpret. In practice, the subset of experimental features which conform to established models of EBIC are interpreted within these models, while anomalous features are ignored or discarded.

One feature of the EBIC signal which we consider here is the internal quantum efficiency (IQE), which is given by the ratio of the collected current to the total electron-hole pair generation rate. We find its maximum can be well below 1 for materials such as CdTe. A reduced IQE in CdTe has also been observed for optical excitation experiments at strongly absorbed wavelengths [2], where most electron-hole pair generation is within the depletion region. A simple estimate reveals that even a small reduction in quantum efficiency within the depletion region implies a large reduction in the mobility-lifetime product $\mu\tau$: The recombination decay length in the presence of the internal field E is $\mu\tau E$. The recombination within the depletion width L_W is therefore $\propto \exp(-L_W/(\mu\tau E))$. For typical internal fields of 10^4 V/cm and depletion widths of 1 μm, a quantum efficiency of 0.9 requires a $\mu\tau$ on the order of $-1/\log(0.9) \times (L_W/E) \approx 10^{-7}$ cm^2/V. For wavelengths with absorption lengths less than 1 μm, the estimate for $\mu\tau$ is even further decreased.

Previously developed models of EBIC experiments assume that $\mu\tau$ is large enough to ensure that all carriers generated in the depletion region are collected (or that the maximum IQE is 1) [3]. We present experimental results for which this condition is not satisfied, and develop a model which includes recombination with the depletion region. We find that the model is consistent with experimental results if we assume a spatially varying $\mu\tau$.

I. Experiment

We first describe the cross-sectional EBIC measurements performed on CdS-CdTe photovoltaic cells. The nominal thickness of the CdTe layer is 2 μm. The samples are prepared by two methods: cleaving and focused ion beam (FIB) milling. The FIB process was performed with 30 keV of Ga beams for a couple of minutes, resulting in a smooth surface over the milling area. Acquisition of EBIC at different electron energies was performed with an Indium contact on n-CdS and a metal probe tip on Au/Cu/p-CdTe. We present results in terms of the EBIC efficiency η, defined as the ratio of the measured current to the total generation rate of electron-hole pairs $G_{\rm tot}$. This generation rate is estimated as [4]:

$$G_{\rm tot} = (1-b)\,\frac{I_{\rm beam} \times E_{\rm beam}}{2.59 \times (E_g/E_0) + 0.17}, \qquad (1)$$

where $I_{\rm beam}$ is the electron beam number current, $E_{\rm beam}$ is the beam energy, E_g is the material bandgap, $E_0 = 1$ eV, and b is the backscattering coefficient (b is determined by Monte Carlo calculations). The beam energy is varied between 5 and 20 keV. We estimate 10 % uncertainty in the measured EBIC ratio. The dominant sources of uncertainty are from the beam current, and from the inhomogeneous material composition which renders our Monte Carlo simulation (performed for pure CdTe) for backscattering approximate, as well as introducing uncertainty in the bandgap used in Eq. 1. We omit the error bars in the data for clarity, but have included them in the fitting parameters' values (all uncertainties are single standard deviations).

Figs. 1(a) and 1(c) show the EBIC efficiency of CdTe solar cells as a function of distance from the CdS-CdTe metallurgical junction, for the cleaved and FIB-prepared samples, respectively (the profile is taken from a single grain). The maximum collection efficiency is clearly less than 1, and varies throughout the depletion region. To estimate the maximum collection efficiency and diffusion length, we first fit the data to the model depicted in Fig. 2. This model is well-established, and has been applied in many previous studies [3], [5].

Briefly, the model assumes a constant collection efficiency ϕ_0 within the depletion width L_W (ϕ_0 is usually taken to

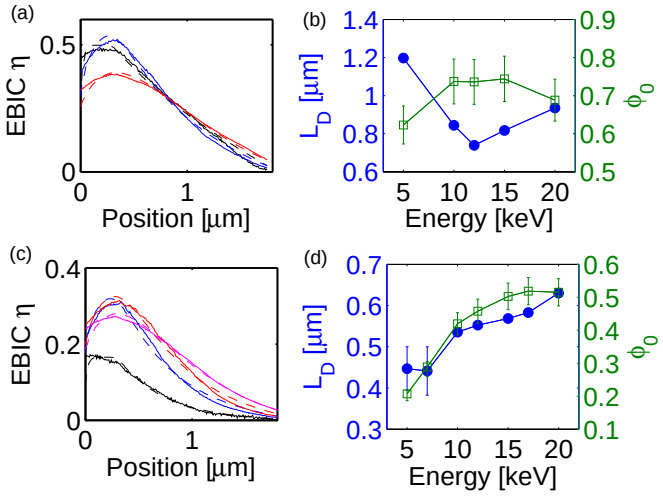

Fig. 1. (a) Solid lines are experimental EBIC profiles for a cleaved CdTe sample. Black, blue, and red correspond to beam energies of 5 keV, 12 keV, and 20 keV, respectively. Dotted lines are model fits. (b) Shows the energy-dependent fit parameters L_D (solid blue dots) and ϕ_0 (open squares). (c) Solid lines are experimental EBIC profiles for a FIB-prepared CdTe sample. Black, blue, red, and magenta correspond to beam energies of 5 keV, 10 keV, 15 keV, and 20 keV, respectively. Dotted lines are model fits. (b) Shows the energy-dependent fit parameters L_D (solid blue dots) and ϕ_0 (open squares).

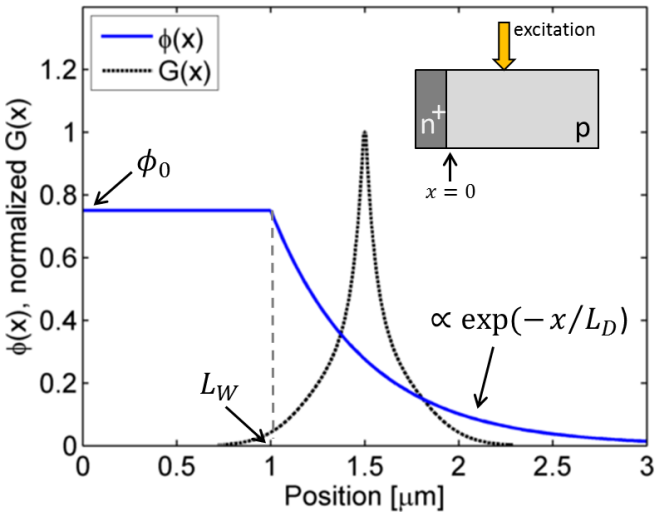

Fig. 2. Schematic of conventional model for side-view EBIC experiments. Inset shows model geometry. The generation profile due to the electron beam is convolved with a collection probability function $\phi(x)$. The generation profiles depend on position and beam energy. Larger beam energies result in larger regions of e-h pair generation.

be 1, here we take it as a free parameter), and a collection probability which decreases exponentially (with a length scale of the minority carrier diffusion length L_D) from the depletion region edge. The model accounts for recombination from the bulk, the exposed surface, and the back contact. The measured EBIC signal for an electron beam positioned at x_0 is the convolution of the collection probability function $\phi(x)$ and the generation profile of electron-hole pairs $G(x, x_0, E_{\text{beam}})$ (note that this profile depends on the beam energy E_{beam}). We use a parameterized form for $G(x, x_0, E_{\text{beam}})$ from Ref. [6], and have checked that it agrees well with Monte Carlo simulations. Fig. 2 shows $G(x, x_0, E_{\text{beam}})$ for $x_0 = 1.5$ μm and $E_{\text{beam}} = 15$ keV.

We perform least-squares fitting of the data of Fig. 1 with the convolution of $\phi(x)$ and $G(x, x_0, E_{\text{beam}})$ to determine L_W, L_D, ϕ_0, and the back contact recombination velocity. L_D and ϕ_0 are energy-dependent because the excitation profile's proximity to the surface (and its associated increased recombination) is energy-dependent. We find a depletion width $L_W = 0.3 \pm 0.03$ μm, which is much lower than the depletion width measured with impedance spectroscopy [7], and lower than the expected value given the nominal sample doping (10^{15} cm^{-3}). The maximum collection efficiency for cleaved samples is shown in Fig. 1b. It is weakly energy-dependent and well below 1. For the FIB-prepared sample (Fig 1d), ϕ_0 and L_D are strongly energy-dependent due to substantial surface damage from the FIB process. Modeling the FIB-induced surface damage is beyond the scope of the present work, and will be presented elsewhere.

The maximum collection efficiency we measure here is consistent with that measured using a top-down EBIC geometry (not shown). We have additionally performed cross-section and top-down EBIC measurements on Si solar cells, and found $\phi_0 = 1$ within uncertainty, and values of L_W and L_D which agree with the expected results. We conclude that the $\phi_0 = 0.7 \pm 0.05$ is indicative of a real material property for this CdTe sample. This indicates that an appropriate model must include recombination within the depletion region.

II. Junction Recombination Model

To inform the construction a model of EBIC which includes junction recombination, we first perform finite-difference simulations on a full p-n junction. The simulation consists of standard coupled continuity equations for electrons and holes, Shockley-Read-Hall recombination (with equal bulk lifetime τ_{bulk} for electrons and holes), and the Poisson equation. Fig. 3 shows the electron and hole densities for a point-source excitation at position $x_0 = 0.35$ μm. We find that the electron and hole densities are equal at the excitation point. Equal electron and hole densities occur when photo-generated minority carrier density exceeds the local equilibrium majority carrier density. We give the conditions for this to hold later; for now we take it as an assumption. This assumption means that the model given only applies to the interior of the depletion region.

We only present analysis of the hole carriers here - the treatment of electrons is identical. For the example shown in Fig. 3, holes are majority carriers to the right of the excitation position, and minority carriers to the left. We find that as minority carriers, holes drift, diffuse, and recombine, while

as majority carriers, holes simply drift. The schematic of the resulting model for holes is shown in Fig. 3b.

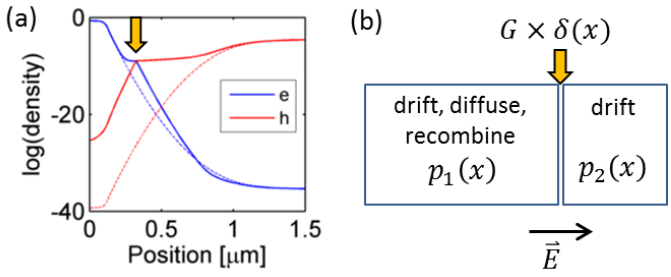

Fig. 3. Model results for a point-source excitation at x=0.35 μm. (a) shows the density of electrons (blue) and holes (red). The dashed lines are the equilibrium densities, while the solid lines are the total densities upon excitation. The model parameters are: doping density of p-type material is $N_A = 10^{15}$ cm^{-3}, majority and minority carrier mobilities are $\mu = 10$ cm^2/V $\cdot$ s, bulk lifetime is $\tau_{\rm bulk} = 50$ ns, bandgap is $E_g = 1$ eV, and dielectric constant $\epsilon = 11\epsilon_0$. The junction is located at $x = 0.12$ μm, and the total system length is 3 μm. (b) shows a schematic of the analytic model which is intended to capture the important physics of the system. This model applies only within the depletion region, where the electron and hole are approximately equal at the excitation point.

For the derivation of an analytic form of the EBIC efficiency, we take the excitation to be a delta-function located at $x = 0$. The equation of continuity for the hole number current J_1 to the left of the excitation is:

$$\partial_x J_1 = \partial_x \left(\mu p_1 E - D\partial_x p_1\right) = -\frac{p}{\tau_{\rm eff}} \tag{2}$$

where D is the hole diffusivity, and $\tau_{\rm eff} = \beta\tau_{\rm bulk}$. β varies between 1 (if $p \ll n$) and 2 (if $p = n$); this follows from the form of Read-Shockley-Hall recombination. We take $\beta = 1.75$ in the reminder of the paper. The continuity equation for holes in the region to the right of the excitation is:

$$\partial_x J_2 = \partial_x \left(\mu p_2 E\right) = 0 \tag{3}$$

We assume that $\partial_x E$ is negligible, or that the electric field varies slowly as compared to the variation of the charge densities. The solution is specified by three boundary conditions: 1. the carrier density goes to 0 as $x \to -\infty$, 2. the density is continuous at the excitation point (assumed to be positioned at $x = 0$), and 3. the current is discontinuous at the delta-function excitation point:

$$p_1(0) = p_2(0) \tag{4}$$

$$J_1(0) - J_2(0) = G \tag{5}$$

The solution $p_1(x)$ which satisfies these conditions is:

$$p_1(x) = \left(\frac{2G}{\mu E\left(x\right)}\right)\frac{1}{1+\sqrt{1+4/f\left(x\right)}} \times \exp\left[-\frac{x\mu E\left(x\right)}{2}\left(1+\sqrt{1+\frac{4}{f\left(x\right)}}\right)\right] \tag{6}$$

where $f\left(x\right) = \left(q\mu\tau_{\rm eff}E\left(x\right)^2\right)/k_{\rm B}T$ (here $k_{\rm B}$ is the Boltzmann constant and T is temperature). In the form given here, we take only the electric field to be spatially-dependent. Later on, we will also allow the parameters μ and τ to vary spatially. The total recombination $R_{\rm tot}$ is the integral of $2p_1(x)/\tau_{\rm eff}$ over x. The factor of 2 arises because an equivalent treatment of electrons applies, doubling the recombination contribution from the holes presented here. The EBIC efficiency is given by $(G_{\rm tot} - R_{\rm tot})$. This leads to the following form of the EBIC response:

$$\eta\left(x\right) = 1 - \frac{R_{\rm tot}}{G_{\rm tot}} = f\left(x\right)\left(\sqrt{1+\frac{4}{f\left(x\right)}} - 1\right) - 1 \tag{7}$$

Eq. 7 is the main theoretical result of the paper.

To test the accuracy of the assumptions underlying the analytical model, we compare its prediction to that of the full simulation of an EBIC experiment. The results are shown in Fig. 4, which indicates that the analytical model works very well. The analytical model breaks down when the densities of electron and holes at the excitation point are not equal. The maximum minority carrier density is given by:

$$p_{\rm max}\left(x\right) = \frac{2G}{\mu E\left(x\right)}\left(\frac{1}{1+\sqrt{1+4/f\left(x\right)}}\right). \tag{8}$$

Eq. (7) applies when $p_{\rm max}\left(x\right)$ exceeds the majority equilibrium density. This condition is satisfied within some interval of the equilibrium "neutral point" - the point with equal electron and hole equilibrium densities. The size of the interval for which the nonequilibrium electron and hole density are equal at the excitation point is determined by G. The precise expression is cumbersome, so we omit it for brevity but note that for uniform excitation density of 1 sun (10^{21} cm^{-3} s^{-1}), the size of this region is on the order of 300 nm around the neutral point. In our EBIC experiments, the local excitation is much more intense than 1 sun. We estimate that the region for which the EBIC excitation leads to equal electron and hole densities at the excitation point covers most of the depletion width.

We note that the signal in Fig. 4 nearly vanishes past $x = 1$ μm. To suppress the maximum collection efficiency, recombination rates must compete with very fast drift velocities, and must therefore be quite short. Away from the internal field, these fast recombination times strongly reduce the signal. This abrupt decay of $\eta(x)$ is at odds with the experimental data of Fig. 1, which show a signal which decays well into the neutral region. This model therefore requires spatially dependent $\mu\tau$ to conform to the experimental data: a $\mu\tau$ which is small near the junction and and increases further into the CdTe layer. A spatial dependence of this quantity is to be expected: SIMS measurements have shown a substantial degree of alloying within 0.2 to 0.4 μm of the metallurgical junction (resulting in a CdTe-CdS alloy)[9], and the distribution of impurities has been observed to vary substantially with position [10].

A. *Junction recombination model - data fits*

We next apply the model developed in the previous section to the experimental data. Using the measured EBIC efficiency

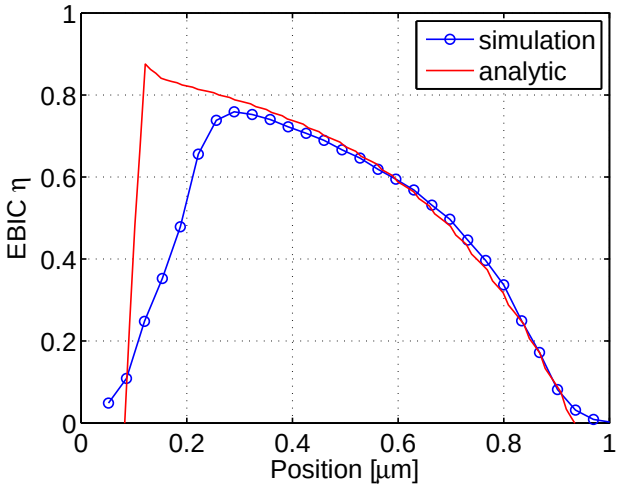

Fig. 4. A comparison between the full simulation results and the analytic formula for the EBIC response. Model parameters are given in the caption of Fig. 3.

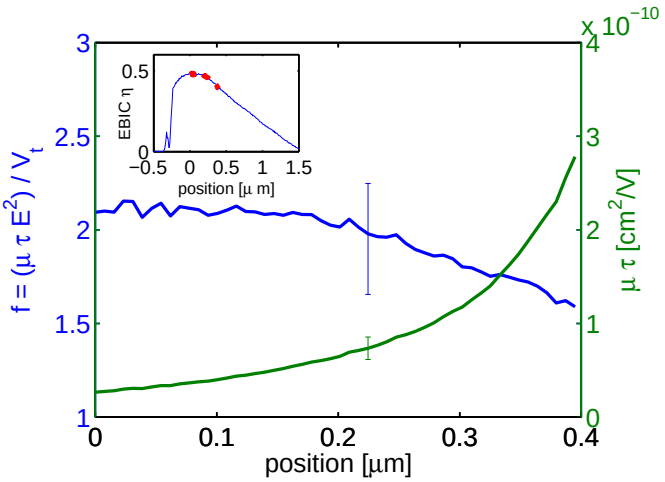

Fig. 5. Application of the analytic EBIC formula to the data of Fig. 1(a). $f(x)$ is shown in blue. In order to extract an estimate of the spatially dependent $\mu\tau$, a standard electric field profile in the junction is assumed(see text for its explicit form), with $V_{\rm bi} = 1.2$ eV, $N_A = 10^{15}$ cm^{-3}. The resulting $\mu\tau$ versus position is shown in green. Representative error bars are shown near $x = 0.22$ μm. The inset shows the EBIC profile, where the red dots indicate the region over which the fitting is performed.

of Fig. 1 together with Eq. (7) enables the determination of the dimensionless $f(x) = \left(\mu\tau qE\left(x\right)^2\right)/k_{\rm B}T$. This is shown in the green curve Fig. 5. The inset shows the EBIC signal profile, and the red portion of the curve is the region to which we apply this model (recall this model applies in the depletion region, where the photogenerated electron and hole densities are approximately equal). If $E(x)$ is known, the spatial profile of $\mu\tau$ can be determined. We assume the spatial profile of $E(x)$ to be the standard form:

$$E\left(x\right) = \frac{N_A}{\epsilon}\left(x - x_p\right) \tag{9}$$

where $x_p = \sqrt{2\epsilon V_{\rm bi}/N_A}$ (here $V_{\rm bi}$ is the built-in potential, and N_A is the acceptor density of p-type region). The general range of values we obtain for $\mu\tau$ for this sample is quite low - on the order of 10^{-10} cm^2/V. This can be compared with measurements using time-of-flight techniques, which estimate $\mu\tau = 10^{-8}$ cm^2/V [8]. Analysis of a different sample is shown in Fig. 6, where we find somewhat larger values of $\mu\tau$. Our initial impression is that these low values indicate that there may be other important physics to consider in analyzing the data. We have additionally considered the effects of high charge injection; this analysis will be presented in a later work, but we find a weak dependence of the signal on beam current, indicating that this is not the likely explanation. We consider this model therefore a first step in understanding all of the features of EBIC data on a quantitative level.

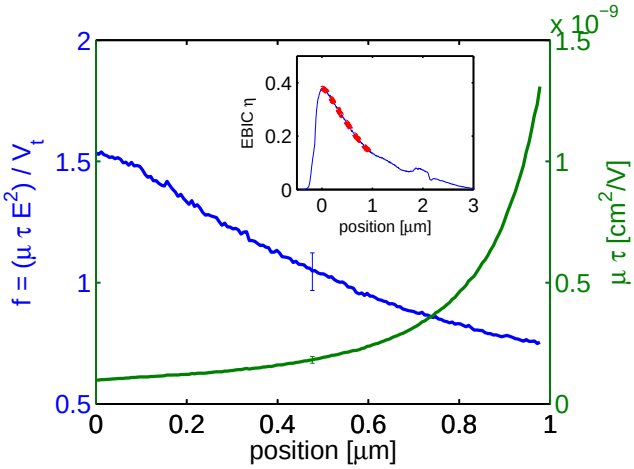

Fig. 6. Application of the analytic EBIC formula to a different CdTe sample (with CdTe layer thickness of 3 μm). $f(x)$ is shown in blue. We assume the standard spatial profile for the electric field (same parameters as in Fig. 5) and extract an estimate of the spatially dependent $\mu\tau$. Representative error bars are shown near $x = 0.5$ μm. The inset shows the EBIC profile, where the red dots indicate the region over which the fitting is performed.

III. Conclusion

We've presented a critical examination of cross-sectional EBIC data on CdS-CdTe photovoltaics, with the main observation that the maximum collection efficiency is less than 100 %. This implies that there is substantial recombination within the depletion region - an effect which is not included in most models of EBIC experiments. We develop a model of EBIC which includes recombination within the depletion region, and find that the model is consistent with experimental results only if there is spatial variation in $\mu\tau$ throughout the depletion region. Application of this model leads to values of $\mu\tau$ which

are quite low (on the order of 10^{-9} cm^2/V), indicating that there may be other important physics that should be included in more refined models of EBIC in complex, polycrystalline materials.

ACKNOWLEDGMENT

H. Yoon acknowledges support under the Cooperative Research Agreement between the University of Maryland and the National Institute of Standards and Technology Center for Nanoscale Science and Technology, Award 70NANB10H193, through the University of Maryland.

REFERENCES

[1] H. P. Yoon, P. M. Haney, D. Ruzmetova, H. Xua, M. S. Leite, B. H. Hamadani, A. Talin, and N. B. Zhitenev, "Local electrical characterization of cadmium telluride solar cells using low-energy electron beam", *Solar Energy Materials and Solar Cells* vol. 117, pp. 499-504, 2013.

[2] O. Vigil-Galán, A. Morales-Acevedo, F. Cruz-Gandarilla, M.G. Jiménez-Escamilla, J. Aguilar-Hernández, G. Contreras-Puente, J. Sastré-Hernández, E. Sánchez-Meza, and M.L. Ramón-Garcia, "CdS layers with different S/Cd ratios in the chemical bath and their relation with the efficiency of CdS/CdTe solar cells", *Thin Solid Films*, vol. 515, pp. 6085-6088, 2007.

[3] C. Donolato, "Evaluation of diffusion lengths and surface recombination velocities from electron beam induced current scans", *Applied Physics Letters*, vol. 43, pp. 120-122, 1983.

[4] C. J. Wu and D. B. Wittry, "Investigation of minoritycarrier diffusion lengths by electron bombardment of Schottky barriers", *Journal of Applied Physics*, vol. 49, pp. 2827-2836, 1978.

[5] Robert Kniese, Michael Powalla, Uwe Rau, "Evaluation of electron beam induced current profiles of Cu(In,Ga)Se2 solar cells with different Ga-contents", *Thin Solid Films* vol. 517, pp. 23572359, 2009.

[6] J. Rechid, A. Kampmann, and R. Reineke-Koch, "Characterising superstrate CIS solar cells with electron beam induced current", *Thin Solid Films*, vol. 361-362, pp. 198-202, 2000.

[7] B.H. Hamadani, J. Roller, P. Kounavis, N.B. Zhitenev, D.J. Gundlach, "Modulated photocurrent spectroscopy of CdTe/CdS solar cellsequivalent circuit analysis", *Solar Energy Materials and Solar Cells*, vol. 116, pp. 126-134, 2013.

[8] S. A. Dinca, E. A. Schiff, B. Egaas, R. Noufi, D. L. Young, and W. N. Shafarman, "Hole drift mobility measurements in polycrystalline CuIn1-xGaxSe2", *Physical Review B* vol. 80, pp. 235201, 2009.

[9] M. Emzianea, K. Durosea, N. Romeob, A. Bosiob,and D.P. Hallidaya, "Effect of CdCl2 activation on the impurity distribution in CdTe/CdS solar cell structures", *Thin Solid Films*, vol. 480, pp. 377-381, 205.

[10] J. Pantoja Enrquez, E. Gômez Barojas, R. Silva González, U. Pal, "S and Te inter-diffusion in CdTe/CdS hetero junction", *Solar Energy and Solar Cells*, vol. 91, pp. 1392-1397, 2007.